Natural Hazards (2021) 107:617–637
https://doi.org/10.1007/s11069-021-04598-9

ORIGINAL PAPER

Extreme value analysis of the typhoon-induced surges on the coastal seas of South Korea

Hyeyun Ku[1] · **Jun Ho Maeng**[1]

Received: 1 June 2020 / Accepted: 21 January 2021 / Published online: 10 February 2021

Abstract

This research mainly focuses on providing new occurrence probabilities of local abnormal sea level rise (SLR) events, i.e., typhoon-induced surge heights, in any given year for the formulation of coastal management and climate change response policies. The 50- and 100-year return period levels of the typhoon-induced surge height on the seas covering the Korean Peninsula are obtained by adopting extreme value analysis with the two most widely applied probability distributions: the generalized extreme value (GEV) and Weibull distributions. The extreme values used in the above extreme value analysis are obtained from the deterministic Sea, Lake, and Overland Surges from Hurricanes model after validation. The statistical estimation is validated by satisfying the hypothesis testing procedure with respect to the form of a probability distribution using chi-squared (Chi-S) and Kolmogorov–Smirnov (K–S) goodness-of-fit tests. The optimal curves consisting of a bird's-eye view of the return period levels of the typhoon-induced surge heights are selected by evaluating the statistical performance indicators of the goodness-of-fit tests, namely the weighted sum χ^2 and supremum D_n of the Chi-S and K–S goodness-of-fit tests, respectively. In this research, the GEV distribution-based fitting curves are selected as the best-fit curves. The increasing pattern of its inverse cumulative distribution function tends to capture the extreme values of the typhoon-induced surge height. Since the numerically obtained typhoon-induced surge heights were employed to visualize the return period levels of the typhoon-induced surges on the seas of Korea, this approach provides more detailed information for the management of SLR-related natural hazards to coastal populations.

Keywords Typhoon-induced surge heights · Meteorological sea level rise · Extreme value analysis · Goodness-of-fit test · SLOSH

✉ Hyeyun Ku
hyeyun.ku@gmail.com; hyku@kei.re.kr

[1] Korea Environment Institute, 370 Sicheong-daero, Sejong 30147, Republic of Korea

1 Introduction

Regarding the climate change induced by both the effects of natural and anthropogenic variabilities, the global mean sea level is rapidly rising in the twenty-first century (Woodworth et al. 2011; IPCC 2013, 2014; Cazenave and Cozannet 2014; Arns et al. 2015; Hamlington et al. 2019). The extreme sea levels arising from climate-related drivers such as storm surges and wind waves over astronomical tides are also similarly increasing with the mean sea level (Lowe et al. 2010; Woodworth et al. 2011; IPCC 2013; Arns et al. 2015). In addition, the typhoons generated by the transformation of a vast amount of heat between oceans and the atmosphere tend to increase in intensity and genesis frequency with increasing global energy under the global warming effect (Knutson et al. 2010). Typhoon-induced surges, which are defined as an abnormal sea level rise (SLR) by typhoon-induced strong winds blowing over shallow and continental shelves, push water to the coast and further lead to an inundation risk in coastal areas, particularly where the population and urbanization has increased (Lowe et al. 2010; Arns et al. 2015; Kim and Cho 2016; Weather Meteorological Organization 2017; Talke and Jay 2020). To prevent meteorological SLR-related risks or to establish climate change adaptation plans, local (extreme) SLR estimation is required as a first step.

The SLR magnitude has been calculated as the rate of change using tidal gauges or satellite altimetry measurements (Woodworth et al. 2011; IPCC 2013; Cazenave and Cozannet 2014; Hay et al. 2015; Hamlington et al. 2019). The data revised by removing the vertical land motion from tide gauge measurements and correcting the effects of the ionospheric and tropospheric delays, instrumental biases, etc., in satellite measurements have been replotted via regression (IPCC 2013; Cazenave and Cozannet 2014; Hay et al. 2015; Kim and Cho 2016). Then, a single SLR rate of change has been mostly obtained and employed in future SLR projection and estimation. The Korea Hydrographic and Oceanographic Agency (KHOA) has reported that the sea level of the seas covering the Korean Peninsula has increased by 2.97 mm/year over the past 30 years (1989–2018). This rate is higher than the global mean SLR rate (KHOA; IPCC 2013).

Even though the extreme SLR pattern follows that of the mean sea level rise (MSLR), the former is mainly driven by meteorological components and bathymetry. In particular, the typhoon-induced surge, which contains uncertainties regarding various processes from its genesis to its extinction, is greatly amplified by waves propagating through narrow and shallow continental shelves (Ku et al. 2019b). For the management of natural hazards such as coastal flooding and strong winds, relevant standards have been mostly estimated in the form of return period levels, with a particular emphasis on the increasing uncertainty due to climate change and human activities (Butler et al. 2007; Toro et al. 2010; Goring et al. 2011; Alam et al. 2018; Ke et al. 2018; Rao et al. 2020).

Frequency analysis has been conducted to relate the magnitude of extreme events such as coastal floods and extreme (the lowest and highest) water levels to their occurrence frequency at given locations. This is based on the extreme value theory that the largest or smallest random variables tend to follow an asymptotic distribution. Various statistical distributions, such as the generalized extreme value (GEV), Weibull, and Gumbel distributions, have been applied to estimate the return period levels of high water levels in rivers, estuaries, and coastal regions, and of flooding and precipitation levels (Kwon et al. 2009; Butler et al. 2007; Arns et al. 2015; Alam et al. 2018). Specifically, the GEV and Weibull distributions have been the most widely employed to fit stationary data sets of wave heights, precipitation, and lowest and highest water levels (Kottegoda and Rosso

1997; Kwon et al. 2009; Butler et al. 2007). In studies estimating the return period levels of the maximum monthly rainfall (Alam et al. 2018) and maximum water level in rivers (Ke et al. 2018), the GEV and Weibull distributions have been adopted to describe the patterns of these extreme values. These estimations have been validated by adopting goodness-of-fit tests such as the chi-squared (Chi-S) and Kolmogorov–Smirnov (K–S) tests and the root-mean-square error (RMSE), which test and reveal whether the data set follows the hypothesized probabilistic distribution.

As a part of assessing the future SLR impact on coastal regions with respect to climate change, this research aims to estimate and update the extreme typhoon-induced SLR in terms of the return period level (or the chance of a certain level being exceeded in any one year) in the seas around the Korean Peninsula. In general, the stationary data for the aforementioned extreme value analysis consist of observations such as those measured at tidal stations for at least 50 years. South Korea possesses a total of 44 tidal stations operated by the KHOA, some of which have observed water levels lower than the threshold. Additionally, estimation of the return period levels by using the above observational data requires spatial interpolation, and regional characteristics such as geographical features cannot be considered. To overcome these drawbacks, this study adopts meteorological extreme sea level data, i.e., the typhoon-induced surge height, obtained with the deterministic Sea, Lake, and Overland Surges from Hurricanes (SLOSH) model after model validation on Korean seas (Jelesnianski et al. 1984; Shaffer et al. 1986; Taylor and Glahn 2008; Glahn et al. 2009; Seo et al. 2018). The return period levels of local extreme sea levels are estimated by adopting the GEV and Weibull distributions. Fitting curves are validated by conducting Chi-S and K–S goodness-of-fit tests. This research also provides the best 50- and 100-year return period levels of local typhoon-induced SLR values and demonstrates the validity of the adaptation of numerically obtained SLR data from the SLOSH model on Korean seas.

2 Methodologies

2.1 Deterministic SLOSH model

In this research, the typhoon-induced surge height above the stationary ocean surface was calculated by the deterministic numerical SLOSH model. This model was developed with the purpose of forecasting real-time storm surges by the National Oceanic and Atmospheric Administration (NOAA), and it has been applied to establish evacuation plans in coastal areas by implementing probabilistic or composite approaches for varying typhoons (Jelesnianski et al. 1984; Shaffer et al. 1986; Taylor and Glahn 2008; Glahn et al. 2009). On estimating the typhoon-induced surge heights, wave–tide–surge nonlinear interaction has been considered for increasing the accuracy (Chen et al. 2017; Hsiao et al. 2019, 2020). Even though the SLOSH model calculates only the wind effect, the SLOSH model has been providing the suitable accuracy in estimating the maximum values of typhoon-induced surges and the wave patterns over the seas around Korean Peninsula (Seo et al. 2018). We adopted the model SLOSH to organize a random variable set of the annual maximum typhoon-induced surges for the probabilistic approach.

The SLOSH model consists of two parts: wind and storm surge ones. The wind model first computes the pressure and wind direction for a stationary, circularly symmetric storm, and these data are used as driving forces in the surge model. (See Seo

et al. 2018; Ku et al. 2019a for the details on verifying the suitability of the wind and storm surge parts on the seas around Korean Peninsula.) The surge model derives the typhoon-induced surge height by solving shallow-water equations conformally transformed from $z=(x, y)$ into $\zeta=(P, Q)$ and then particularized onto a polar frame of reference given by (please refer to Jelesnianski et al. 1992; Kim et al. 1996 for details):

$$\zeta = P + iQ = \ln\left(\frac{r}{R_0}\right) + i\theta \tag{1}$$

where R_0 is a convenient scale. The final form of the governing equations is expressed as:

$$\frac{\partial U}{\partial t} = -g(D+h)\left[B_r\frac{\partial h}{\partial P} - B_r\frac{\partial h}{\partial Q}\right] + f\left(A_r V + A_i U\right) + \left[\mathrm{Re}\left(\frac{\partial z}{\partial \zeta}\right)^*\right]T_x - \left[\mathrm{Re}\left(\frac{\partial z}{\partial \zeta}\right)^*\right]T_y, \tag{2}$$

$$\frac{\partial V}{\partial t} = -g(D+h)\left[B_r\frac{\partial h}{\partial Q} - B_r\frac{\partial h}{\partial P}\right] + f\left(A_r V + A_i U\right) + \left[\mathrm{Re}\left(\frac{\partial z}{\partial \zeta}\right)^*\right]T_x + \left[\mathrm{Re}\left(\frac{\partial z}{\partial \zeta}\right)^*\right]T_y, \tag{3}$$

subject to:

$$\frac{\partial h}{\partial t} = -\left|\frac{\partial \zeta}{\partial z}\right|^2 \cdot \left(\frac{\partial U}{\partial P} + \frac{\partial V}{\partial Q}\right) \tag{4}$$

where U and V are volume transport components on the polar frame of reference, D is the quiescent water level relative to a common datum, h is the wave height above the reference datum, h_0 is the hydrostatic water level, and f is the Coriolis parameter. Parameters T_x and T_y indicate the atmospheric forcing terms defined on the Cartesian coordinate system as follows:

$$T_x = g(D+h)\left(B_r\frac{\partial h_0}{\partial x} - B_i\frac{\partial h_0}{\partial y}\right) + C_r\tau_x - C_i\tau_y, \tag{5}$$

$$T_y = g(D+h)\left(B_r\frac{\partial h_0}{\partial y} - B_i\frac{\partial h_0}{\partial x}\right) + C_r\tau_y - C_i\tau_x. \tag{6}$$

In Eqs. (3)–(6), the bottom stress coefficients of A_r, A_i, B_r, B_i, C_r and C_i consist of real and imaginary components with subscripts r and i, respectively. These surface stresses over water bodies are usually obtained from meteorological sources, i.e., the wind at a height of 10 m above the sea, by computing the pressure and wind direction for a stationary and circularly symmetric storm defined as:

$$\frac{1}{\rho_a}\frac{\mathrm{d}p(r_t)}{\mathrm{d}r_t} = \frac{k_s V^2}{\sin\phi} - V\frac{\mathrm{d}V}{\mathrm{d}r_t}, \tag{7}$$

$$\frac{1}{\rho_a}\frac{\mathrm{d}p}{\mathrm{d}r_t}\cos\phi = fV + \frac{V^2}{r_t}\cos\phi - V^2\frac{\mathrm{d}\phi}{\mathrm{d}r_t}\sin\phi + k_n V^2, \tag{8}$$

where the wind speed profile is given by:

$$V(r_t) = V_R \frac{2Rr_t}{R^2 + r_t^2}, \tag{9}$$

where r_t is the distance from the storm center to any given location within the circularly symmetric storm, $p(r_t)$ is the pressure, $\phi(r_t)$ is the inflow angle across circular isobars toward the storm center, $V(r_t)$ is the wind speed, and k_s and k_n are empirical surface friction coefficients. The maximum wind speed and its radius are written as C_R and R, respectively.

2.2 Probability distribution function

2.2.1 Generalized extreme value (GEV) distribution

The GEV distribution is a flexible three-parameter model that identifies the frequency distribution of extreme events, i.e., a set of random variables $q_i (i = 1, \ldots, l)$. The cumulative distribution function (CDF) of the GEV distribution is given by:

$$F_Q(q) = \exp\left\{-\left[1 - \frac{\kappa(q-\epsilon)}{\alpha}\right]^{1/\kappa}\right\}. \tag{10}$$

The three parameters are α, ϵ, and κ, which correspond to scale, location, and shape parameters, respectively. These are estimated by applying maximum likelihood estimation (MLE). The given return period values of exceedance that are on the inverse GEV CDF function (also as known as quantile function) are as follows:

$$q(T) = \xi_{1-\frac{1}{T}} = \epsilon + \frac{\alpha}{\kappa}\left[1 - \left(\ln\frac{T}{T-1}\right)^{\kappa}\right], \tag{11}$$

where $q_{max}(T)$ is the required design value over return period T in year and ξ are the inverse values of the GEV CDF form.

2.2.2 Weibull distribution

The Weibull distribution is one of the Type III extreme value distributions (also written as EV3) and is the most widely used with respect to smallest-extreme problems, such as stream flows and water levels (Kottegoda and Rosso 1997; Alam et al. 2018; Ke et al. 2018). Its CDF is given by:

$$F_Q(q) = 1 - \exp\left[-\left(\frac{q}{\lambda}\right)^{\beta}\right], \quad q \geq 0 \tag{12}$$

where λ and β are location and shape parameters, respectively. As the application of the EV3 (third asymptotic) distribution, these parameters are $\lambda \geq 0$ and $\beta > 0$ (Kottegoda and Rosso 1997), and they are estimated via MLE. From the inverse form of the Weibull distribution, the quantile function $q(T)$ is represented by:

$$q(T) = \xi_{1-\frac{1}{T}} = -\lambda\left[\ln\left(\frac{1}{T}\right)\right]^{\frac{1}{\beta}}. \tag{13}$$

2.3 Statistical performance indication

In this study, we estimated the return period values using two types of probability distribution functions: the GEV and Weibull distributions. It is necessary to ascertain whether these distributions are suitable. In this study, we adopted Chi-S and K–S goodness-of-fit tests. Here, in this subsection, these goodness-of-fit tests are briefly explained.

2.3.1 Chi-square goodness-of-fit test

The Chi-S goodness-of-fit test is one main method of comparing observed (or numerically estimated) and hypothetical (or statistically obtained) frequencies through full or specified classes (Kottegoda and Rosso 1997). The weighted sum of the squared differences between these frequencies is as follows:

$$\chi^2 = \sum_{i=1}^{l} \frac{\left(O_i - E_i\right)^2}{E_i}. \tag{14}$$

In Eq. (14), O_i is the observed frequency and E_i is the expected frequency. To satisfy the hypothetical frequencies that are acceptable, the weighted sum χ^2 should be less than that of a critical value of a χ_v^2 distribution. This distribution depends on the degrees of freedom, $v = l - 1 - k$, where k is the number of estimation parameters.

2.3.2 Kolmogorov–Smirnov goodness-of-fit test

The K–S goodness-of-fit test is a nonparametric, empirical distribution function test based on the CDF. It involves the supreme class of the distances between the theoretical and empirical CDFs (Kottegoda and Rosso 1997; Dufour et al. 1998; Alam et al. 2018).

$$D_n = \sup_i \left| F_n(q) - F_Q(q) \right|, \tag{15}$$

where $F_Q(q)$ is a completely specified theoretical continuous CDF and $F_n(q)$ is the empirical distribution function given as follows:

$$F_n(q) = \begin{cases} 0 & \text{for } q < q_1 \\ k/l & \text{for } q_i \le q < q_{i+1} \\ 1 & \text{for } q \ge q_l. \end{cases} \tag{16}$$

Here, i means the sequence of the random variables $q_i (i = 1, \ldots, l)$.

For the K–S goodness-of-fit test, the critical values correspond to the level of significance φ. In this paper, the level of significance is set as $\varphi = 0.05$, and the critical value of the K–S goodness-of-fit test is defined as $D_{n,\varphi} = 1.36/\sqrt{(l)}$, where the sample size l is larger than 40.

2.4 Data for the extreme value analysis

As previously mentioned in Sect. 2.1, the deterministic SLOSH model is employed to establish a data set of the meteorological SLR induced by typhoons over the Korean input

basin covering the Korean Peninsula (Seo et al. 2018; Ku et al. 2019a). According to previous studies on the application of the SLOSH model to the Korean Peninsula (Seo et al. 2018; Ku et al. 2019a), the estimation of local and meteorological SLR values with the SLOSH model falls within approximately ± 20 to ± 50% error bounds over and under the threshold of the typhoon-induced surge height, which is approximately 3 m (10 ft). Again, these error bounds are based on previous studies on the SLOSH model accuracy (Jelesnianski et al. 1992; Glahn et al. 2009).

The meteorological SLR values for the extreme value analysis were obtained in regard to the historical typhoons affecting the Korean Peninsula from 1951 to 2017. A total of 199 typhoons impacted the Korean Peninsula or the Seas of Korea. These typhoons are listed in Table 1, with the same ID as that assigned by the Regional Specialized Meteorological Center (RSMC). The first two digits indicate the calendar year, followed by a 2-digit serial number only for those storms stronger than a tropical storm. No typhoon affected Korea in 1988, 2001, and 2009. The historical typhoon input data for the SLOSH model were established by adopting the best-track data of the RSMC. Their 6-hourly data were converted into hourly tracks for 100 h, at least 48 and 12 h before and after typhoon landing, respectively. The typhoon input data consisted of the latitude and longitude of the typhoon center in degrees, the moving speed in mph, the moving direction in degrees, the minimum sea level pressure (MSLP) in mb, and the radius of the maximum sustained wind speed (RMW) in mph.

For the extreme value analysis, the annual maximum values of the typhoon-induced surge heights were sampled at each grid point of the Korean input basin for the SLOSH model. The goodness-of-fit tests were conducted at a total of 44 tidal stations of the KHOA including those shown in Fig. 1. The tidal stations are shown in Fig. 1 with respect to the seas: the red asterisks, magenta squares, coral diamonds, and green circles represent the Yellow Sea, South Sea, East Sea, and Jeju Island, respectively. The identification numbers attached to the tidal stations indicate their location, i.e., Incheon (78), Yeosu (9), Masan (219), Ulsan (5), Pohang (4), and Seogwipo (14), which were chosen to visualize the results such as the fitting curves and CDFs. Note that the Busan and Tongyeong tidal stations are depicted to examine the suitability of the return period levels of the typhoon-induced surges obtained from the deterministic SLOSH model in Sect. 4.

3 Results

3.1 Maximum envelope of water (MEOW)

The MEOW is a set of maximum water heights at each grid point. Previous studies (Seo et al. 2018; Ku et al. 2019a, b) have calculated the typhoon-induced surges on the Korean input basin; the MEOW occurs when a typhoon approaches the Korean Peninsula by piling up the water surface along shallow and continental shelves. Figure 2 shows the MEOWs for the historical typhoons of Sarah (5914), Thelma (8705), Maemi (0314), and Bolaven (1215), which penetrated the south coast of Korea, Straits of Korea, and the Yellow Sea. Additionally, these typhoons reached the 4–5 Saffir–Simpson scale in their life cycle, as underlined in Table 1. As typhoons Sarah (5914), Thelma (8705), and Maemi (0314) passed directly through the southern coastal shelves and Straits of Korea, the highest SLR occurred along both sides of the typhoon path, which was then amplified on the southern coasts. In contrast, typhoon Bolaven (1215) penetrated the Yellow Sea, and the highest sea

Table 1 Historical typhoons considered to calculate the typhoon-induced surge heights

Scale number[a] (category)	Central pressure (mb)	International number ID
1	≥ 980	5114, 5201, 5204, 5302, 5309, 5407, 5508, 5613, 5904, 5911, 5913, 6110, 6205, 6305, 6407, 6409, 6513, 6518, 6617, 6911, 7004, 7120, 7305, 7411, 7502, 7611, 7612, 7615, 7707, 7803, 8007, 8104, 8120, 8412, 8505, 8708, 8906, 9007, 9219, 9305, 9407, 9211, 9507, 9905, 9908, 9917, 0006, 0304, 0407, 0610, 0807, 1004, 1009, 1207, 1304, 1412, 1703
2	965–979	5304, 5611, 5906, 6006, 6015, 6016, 6209, 6615, 6710, 6804, 6807, 7128, 7209, 7310, 7808, 7811, 7818, 8012, 8105, 8110, 8211, 8219, 8509, 9005, 9015, 9112, 9306, 9413, 9414, 9809, 9907, 0004, 0012, 0410, 0415, 1105, 1210, 1213
3	945–964	5209, 5415, 5609, 5909, 6104, 6304, 6309, 6405, 6411, 6816, 7002, 7011, 7207, 7220, 7408, 7416, 7609, 7617, 7910, 7911, 8013, 8118, 8213, 8403, 8410, 8508, 8513, 8520, 8605, 8613, 8616, 9117, 9503, 9612, 9711, 9719, 0014, 0205, 0209, 0215, 0306, 0310, 0603, 0705, 1007, 1109, 1411, 1511, 170
4	920–944	5111, 5115, 5412, 5507, 5522, 5612, 5705, 5707, 5819, 6123, 6210, 6217, 6515, 6618, 7009, 7119, 7303, 7505, 8210, 8310, 8705, 8712, 8911, 9109, 9210, 9307, 9313, 9429, 9514, 9606, 9709, 9810, 9918, 0416, 0418, 0514, 0704, 0711, 1324, 1408, 1419, 1509, 1515, 1718
5	< 920	5914, 6118, 7709, 9019, 0314, 0613, 1215, 1216, 1618

The typhoons are written in the form of RSMC best-track data, i.e., the first two digits indicate the calendar year, and the subsequent two digits of the serial number ID indicate any storms of tropical storm intensity or higher

[a]Please refer to the Saffir–Simpson Hurricane Damage Potential Scale for details (Ahrens 2005)

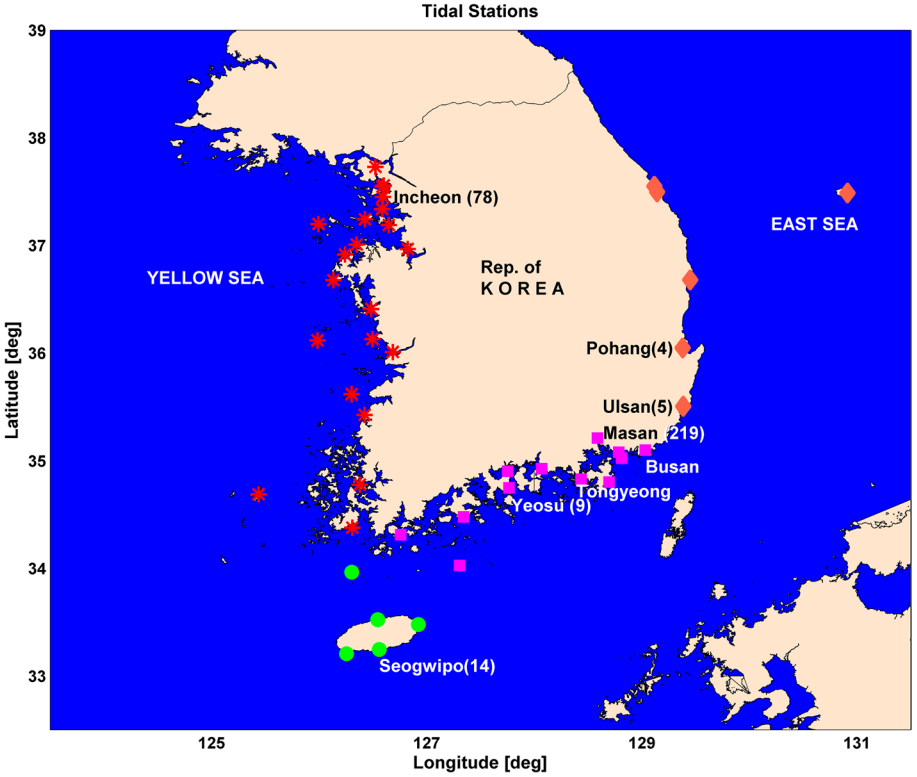

Fig. 1 Locations of the tidal stations (operated by the Korea Hydrographic and Oceanographic Agency) in South Korea. The red asterisks, magenta squares, coral diamonds, and green circles are the tidal stations located in the Yellow Sea, South Sea, East Sea, and Jeju Island, respectively

level occurred along the west coast. The waves generated by the strong winds within the typhoon (at times decreasing to a tropical depression while approaching Korea) were transported from their origin (Boccotti 2000) toward the western coast of Korea.

Figure 2 also shows the highest SLR due to a single typhoon event on the coastal shelves along the typhoon path. Even though the MEOWs of all 199 historical typhoons are not addressed in this article, it is supposed that the maximum values of the MEOWs would reach approximately 3 m due to typhoons of 4 scale or greater, especially along the west and south coasts of Korea. In this research, for the extreme value analysis, these MEOWs are classified by the year and sorted in ascending order. These annual maximum values of the typhoon-induced surge heights are shown in Fig. 3, and they are adopted as random variables to fit curves with the GEV and Weibull probability distribution functions.

3.2 Probability distributions of the typhoon-induced surge heights

Figure 3 depicts the best-fit curves of the GEV and Weibull distributions at the six tidal stations of Incheon (78), Yeosu (9), Masan (219), Ulsan (5), Pohang (4), and Seogwipo (14) with 95% confidence intervals corresponding to the lower and upper confidence limits C_l and C_u which satisfy $\Pr\left[C_l < \theta < C_u\right] = 1 - \alpha$) for $\alpha = 0.05$ by using Walda method. (See

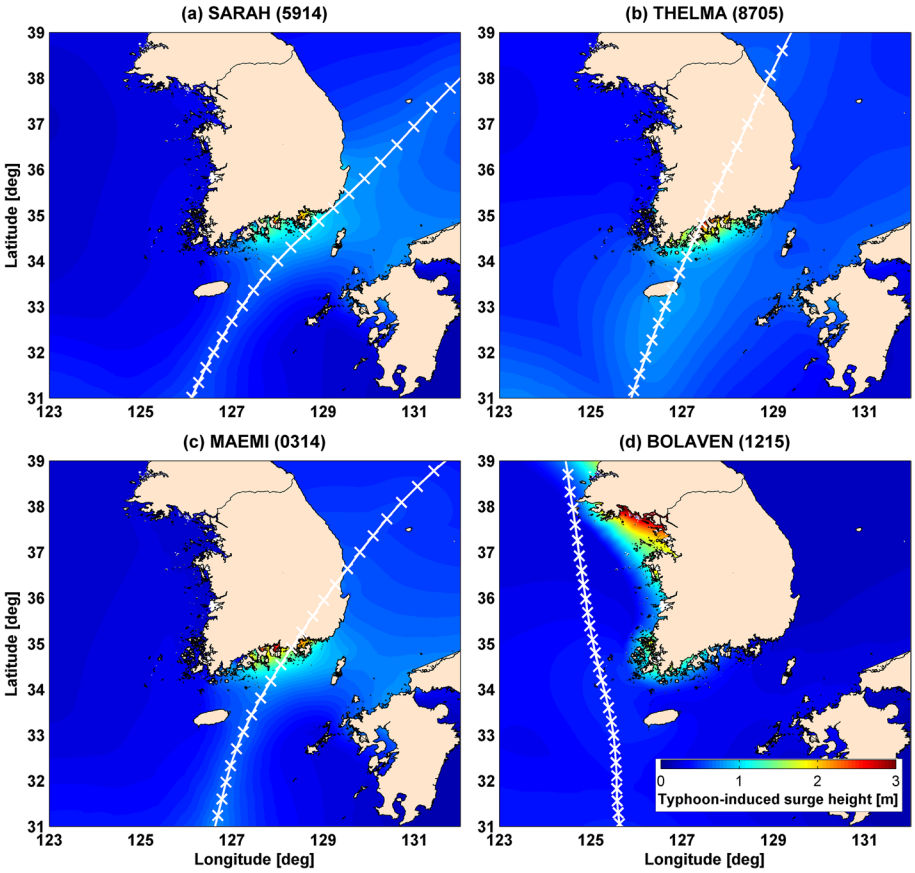

Fig. 2 Maximum envelope of water of typhoons **a** Sarah (5914), **b** Thelma (8705), **c** Maemi (0314), and **d** Bolaven (1215). The typhoon paths are shown with white straight lines and hourly 'x' positioning marks

Kottegoda and Rosso 1997 for details.) Both the GEV and Weibull distributions follow the annual maximum typhoon-induced surge heights well, especially for typhoon-induced surges below 0.8 m, i.e., at the Pohang and Seogwipo tidal stations with the converging pattern. On the GEV distribution, these converging patterns are depicted by negative shape parameters κ shown in Table 2 satisfying the sufficient condition for convergence of bounded random variables (Kottegoda and Rosso 1997). The relatively large shape parameters β of the Weibull distribution of the Pohang and Seogwipo tidal stations resulted in decreasing rates of changes in the typhoon-induced surge heights. But these converging patterns of the GEV distribution do not capture the highest typhoon-induced surges.

At the other tidal stations, the annual maximum values beyond the threshold of a 1-m typhoon-induced surge were recorded, i.e., at the Incheon, Yeosu, Masan, and Ulsan tidal stations in Fig. 3. The positive shape parameters κ and β in GEV and Weibull distributions in Table 2 describe that these stations have recorded strictly monotonic and continuous typhoon-induced surge heights up to the largest values. But only on the GEV fitting curve, the rate of change has increased and led to a sharp increase in its fitting curve. This resulted in different patterns of the GEV and Weibull distribution curves. Even though both curves

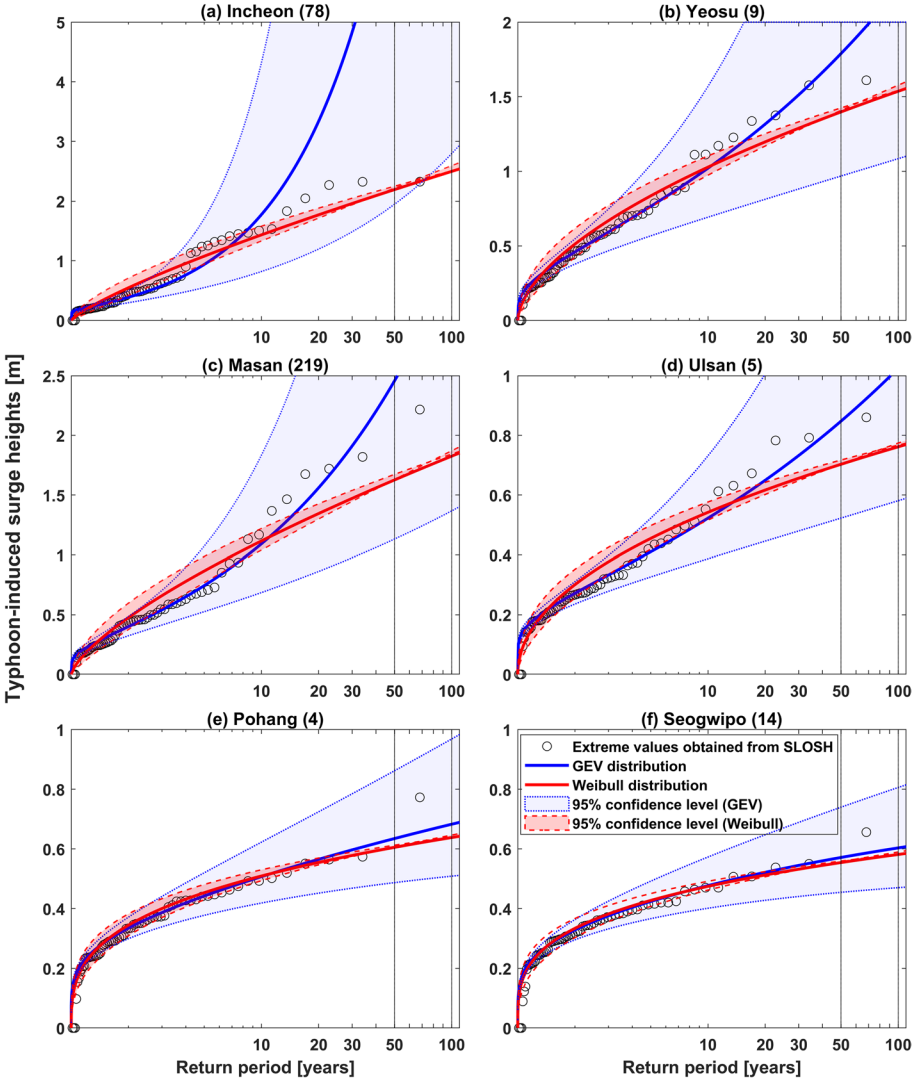

Fig. 3 Best-fit curves for the generalized extreme value (GEV) and Weibull distributions at six tidal stations, **a** Incheon, **b** Yeosu, **c** Masan, **d** Ulsan, **e** Pohang, and **f** Seogwipo. The red and blue straight lines are the GEV and Weibull distributions, respectively. The circles are the annual maximum values of the MEOWs of all 199 historical typhoons

underestimate the annual maximum typhoon-induced surge for return periods shorter than 10 years, the increasing rate of change of the GEV distribution results in its curve approaching the annual maximum values at long return period. These differences are also observed in Figs. 4 and 5. Figure 4 shows the empirical CDFs $F_n(q)$ and those of the probability distributions $F_Q(q)$ with 95% confidence intervals. The increasing rate of the change of the GEV distribution leads to an overestimation of the typhoon-induced surge for long return periods due to the convergence point (i.e., where the slope equals 0) occurring later

Table 2 Estimate of parameters for GEV and Weibull distribution at Incheon(78), Yeosu(9), Masan(219), Ulsan(5), Pohang(4), and Seogwipo(14) tidal stations

Probability distribution	Incheon (78)	Yeosu (9)	Masan (219)	Ulsan (5)	Pohang (4)	Seogwipo (14)
GEV						
Shape, κ	0.4	0.1	0.2	0.0	−0.2	−0.3
Scale, α	0.3	0.3	0.2	0.1	0.3	0.4
Location,ϵ	0.3	0.4	0.3	0.2	0.3	0.3
Weibull						
Location, λ	0.7	0.6	0.6	0.4	0.4	0.4
Shape, β	1.2	1.7	1.4	2.0	3.1	3.4

on the x-axis than that of the Weibull distribution. Figure 5 indicates the 50- and 100-year return period levels at 44 tidal stations. Some of the estimated frequencies of the 50- and 100-year return periods are much higher in the GEV distribution, especially at the tidal stations along the west coast. Additionally, these values result in much higher estimations of the annual maximum variables than those with the Weibull distribution. The decreasing or converging rate of change, particularly of the Weibull distribution along most coasts, results in a few gaps between the 50- and 100-year return period levels.

3.3 Statistical performance indicators

The hypothesis testing procedure related to the form of the probability distribution is the first step assessing acceptance or rejection of the null hypothesis that the random variables have the GEV or Weibull distribution with the specified coefficients. Here, this is quantified by statistical performance indicators such as the weighted sum χ^2 of the Chi-S test and supremum $D_{n,\varphi}$ of the K–S test. There are two objectives to the performance examination of statistical analysis. First, it is verified whether the probabilistic distributions are suitable. The second objective is to provide criteria and guidance for the determination of better fitting curves.

Here, we first examine the performance of the statistical analysis in verifying the suitability of the two probabilistic distributions. The Chi-S and K–S goodness-of-fit tests ascertain the acceptance of the null hypothesis by weighted sum χ^2 and supremum $D_{n,\varphi}$ values that are lower than their critical values. In this research, the critical values for the Chi-S and K–S goodness-of-fit tests are $\chi^2_v = 81.4$ and $D_{n,\varphi}=0.17$, respectively, at a significance level of $\varphi=0.05$ (Kottegoda and Rosso 1997; Panik 2005). Figures 6, 7 and Table 3 show the values of the Chi-S and K–S goodness-of-fit tests. At all tidal stations, the values of both goodness-of-fit tests are lower than their critical values. Therefore, the null hypothesis is accepted at all tidal stations regarding both the GEV and Weibull distributions.

In regard to the critical values, the lower the weighted sum χ^2 and supremum D_n values are, the better the agreement between the curves is. Figure 6 shows that the Weibull distribution is better in terms of the Chi-S goodness-of-fit test, while Fig. 7 shows that the GEV results are better by the K–S test. Table 3 also summarizes the differences in the goodness-of-fit test values between the two probabilistic distributions. In the Chi-S test, the differences are in the range of $0.03 \le \chi^2 \le 0.69$, and the Weibull distribution is better except for tidal station 282, which is located on the northernmost coast of South Korea in the Yellow Sea. The K–S test values are in the range

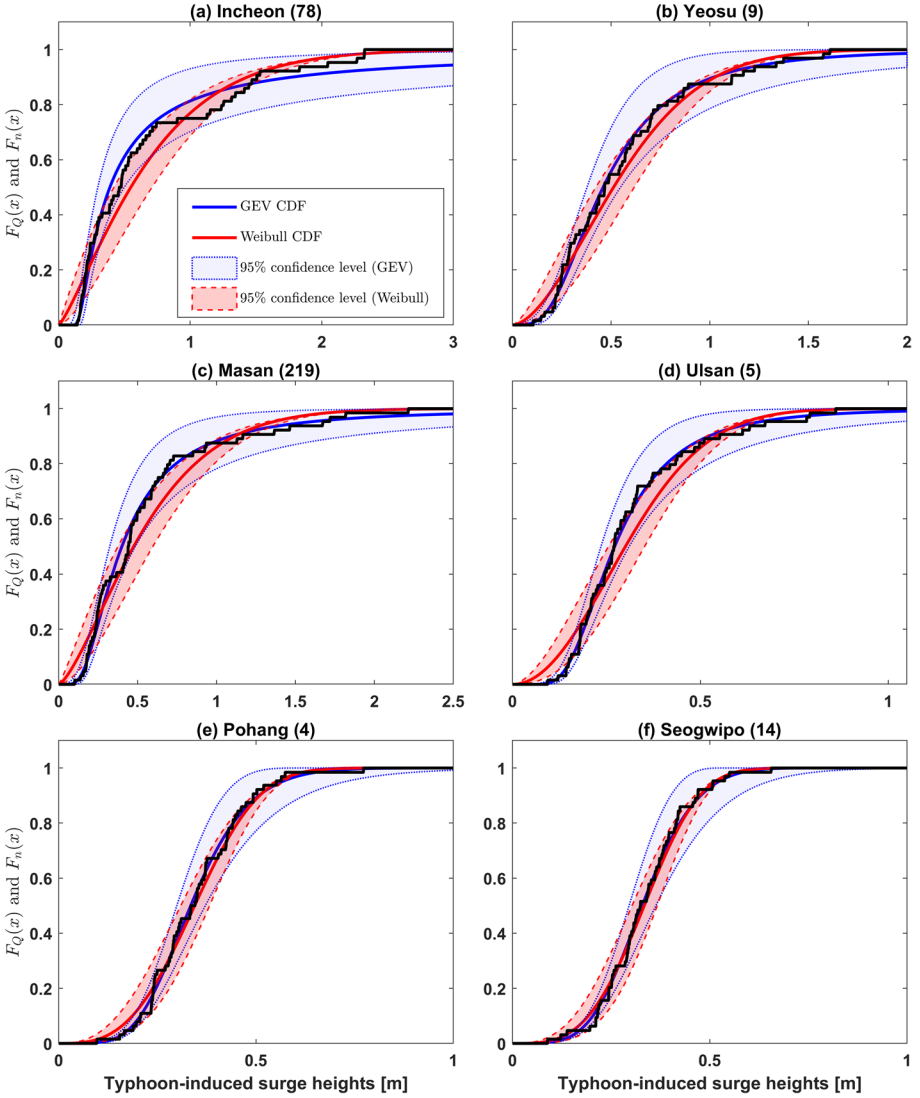

Fig. 4 Cumulative distribution function (CDF) of the GEV and Weibull distributions at the 95% confidence level based on the empirical CDF (the black straight line). The blue and red straight lines indicate the GEV and Weibull distributions, respectively. The dotted and dashed lines indicate their 95% confidence levels

of $0 \le D_n \le 0.03$, and the GEV distribution attains a better performance in estimating the return period level. To select the best distribution for variable fitting purposes, Alam et al. (2018) established a ranking system that ranked goodness-of-fit test results in descending order with respect to the probabilistic distribution and summed these ranked values. The smaller the sum is, the better the curve fit is. Even though this research evaluated just two probabilistic distributions by two goodness-of-fit tests, in

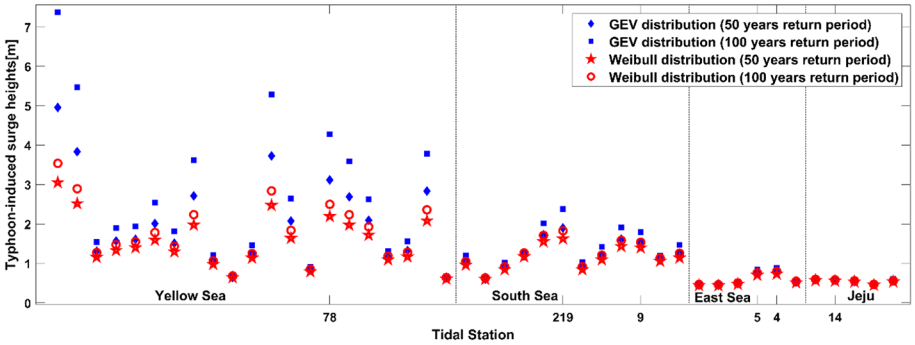

Fig. 5 Estimated frequencies of the 50- and 100-year return period levels by the generalized extreme value (GEV) and Weibull distributions at 44 tidal stations. The blue diamonds and squares and red pentagrams and circles represent the 50- and 100-year return period levels, respectively, obtained by the GEV and Weibull distributions, respectively

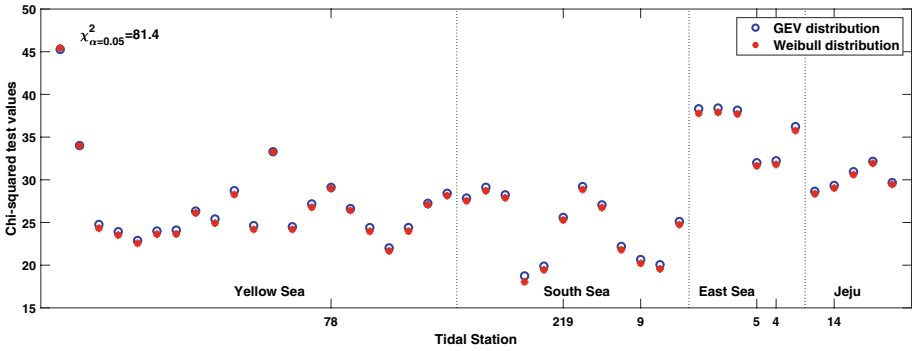

Fig. 6 Chi-squared goodness-of-fit test results at 44 tidal station in South Korea

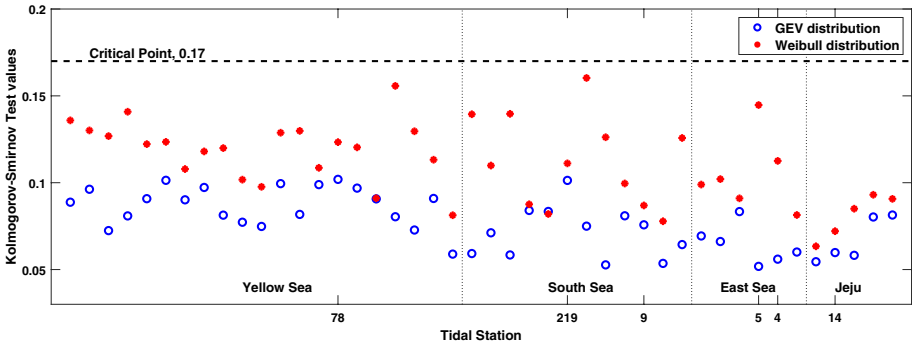

Fig. 7 Kolmogorov–Smirnov goodness-of-fit test results at 44 tidal station in South Korea

applying the above ranking system (Alam et al. 2018), the GEV distribution is better to estimate the probability of exceeding a certain level in any given year because of the ranking score of tidal station 282.

Table 3 Statistical performance indicators, i.e., the weighted sum χ^2 of the chi-squared goodness-of-fit test and the supremum D_n of the Kolmogorov–Smirnov goodness-of-fit test at 44 tidal stations

Probability Distribution		Generalized Extreme Value (GEV)				Weibull			
Seas	Station ID no.	χ^2		D_n		χ^2		D_n	
Yellow Sea	282	45.27	●	0.09	▲	45.44		0.14	
	462	34.01		0.10	▲	33.98	●	0.13	
	356	24.77		0.07	▲	24.33	●	0.13	
	220	23.92		0.08	▲	23.53	●	0.14	
	15	22.89		0.09	▲	22.56	●	0.12	
	20	24		0.10	▲	23.63	●	0.12	
	458	24.11		0.09	▲	23.65	●	0.11	
	211	26.33		0.10	▲	26.10	●	0.12	
	21	25.41		0.08	▲	24.92	●	0.12	
	343	28.73		0.08	▲	28.27	●	0.10	
	208	24.63		0.07	▲	24.19	●	0.10	
	365	33.29		0.10	▲	33.24	●	0.13	
	364	24.5		0.08	▲	24.19	●	0.13	
	17	27.17		0.10	▲	26.78	●	0.11	
	78	29.11		0.10	▲	28.97	●	0.12	
	459	26.63		0.10	▲	26.41	●	0.12	
	241	24.4		0.09	▲	23.96	●	0.09	
	276	22.02		0.08	▲	21.66	●	0.16	
	457	24.4		0.07	▲	23.97	●	0.13	
	50	27.24		0.09	▲	27.06	●	0.11	
	16	28.42		0.06	▲	28.14	●	0.08	
South Sea	7	27.86		0.06	▲	27.53	●	0.14	
	10	29.12		0.07	▲	28.71	●	0.11	
	275	28.24		0.06	▲	27.88	●	0.14	
	92	18.74		0.08	▲	18.05	●	0.09	
	60	19.88		0.08	-	19.45	●	0.08	-
	219	25.59		0.10	▲	25.28	●	0.11	
	6	29.21		0.07	▲	28.86	●	0.16	
	460	27.06		0.05	▲	26.74	●	0.13	
	465	22.2		0.08	▲	21.80	●	0.10	
	9	20.66		0.08	▲	20.21	●	0.09	
	44	20.05		0.05	▲	19.55	●	0.08	
	8	25.11		0.06	▲	24.75	●	0.13	
East Sea	461	38.32		0.07	▲	37.78	●	0.10	
	2	38.4		0.07	▲	37.90	●	0.10	
	3	38.15		0.08	▲	37.71	●	0.09	
	5	32		0.05	▲	31.63	●	0.14	
	4	32.23		0.06	▲	31.79	●	0.11	
	218	36.23		0.06	▲	35.76	●	0.08	
Jeju	238	28.65		0.05	▲	28.36	●	0.06	
	14	29.34		0.06	▲	29.02	●	0.07	
	237	30.95		0.06	▲	30.61	●	0.09	
	13	32.16		0.08	▲	31.93	●	0.09	
	12	29.67		0.08	▲	29.46	●	0.09	

Red disk (●) and blue triangles (▲) are marking higher rank of the statistical performances

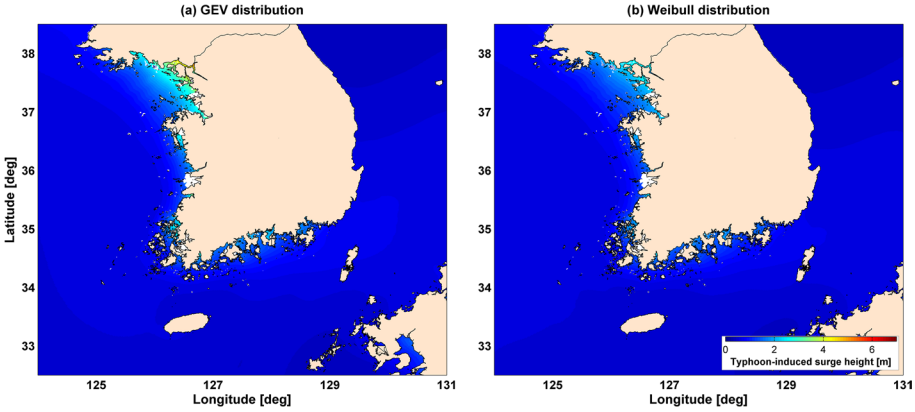

Fig. 8 Bird's-eye view of the 50-year return period levels of the typhoon-induced surge height by the **a** GEV and **b** Weibull distributions around the Korean Peninsula

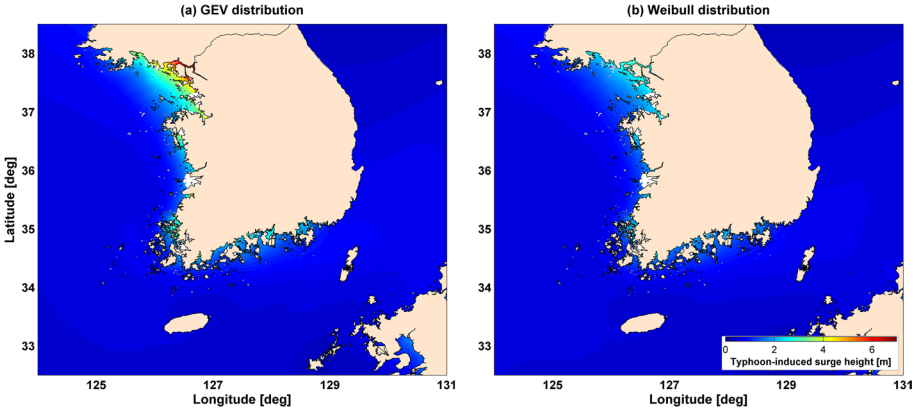

Fig. 9 Bird's-eye view of the 100-year return period levels of the typhoon-induced surge height by the **a** GEV and **b** Weibull distributions around the Korean Peninsula

4 Discussion of the return period levels of the typhoon-induced surges

Figures 8 and 9 show a bird's-eye view of the 50- and 100-year return period levels, respectively, of the typhoon-induced surge height. The highest and relatively higher return period levels of the typhoon-induced surge height occur along the west and south coasts, respectively, based on the GEV distribution. The increasing rates of change shown in Figs. 3 and 4 resulted in higher return period levels. Additionally, comparing the 50- and 100-year return period levels of the typhoon-induced surge height, the converging pattern of the Weibull distribution resulted in a relatively gradual increase. The differences obtained from the probability distribution reached approximately 4 m (please refer to Fig. 5 for details) at the 100-year recurrence level.

The relatively higher return levels of the typhoon-induced surge height occurring along the south coast resulted from the historical typhoons frequently penetrating the south coast and Straits of Korea and the geographical features of the narrow and long channels. In

particular, Masan Bay with the Masan (219) tidal station (please refer to Fig. 1 for the locations of the tidal stations) exhibits these geographical features. These factors amplified the waves generated by the typhoon-induced strong winds and delivered them to the inside of the bay (Ku et al. 2019a).

In the case of the east coast, the return period water levels are much lower than those along the west and south coasts. The typhoon-induced SLR values of the MEOW shown in Fig. 2 even smoothly decrease along the north direction. In general, typhoons lost energy when moving on land in the east direction, and they faded out. This resulted in relatively lower typhoon-induced winds and surge heights. In most cases, the east coast is not directly affected by typhoons.

In Sect. 3.3, the comparison of the weighted sum χ^2 of the Chi-S goodness-of-fit test and the supremum D_n of the K–S test revealed that the GEV distribution attained a better performance in estimating the return period level of local typhoon-induced SLR values because of its lower goodness-of-fit test values. Particularly, the GEV distribution, i.e., the increasing slopes of the best-fit curves, as shown in Fig. 3, leads to higher typhoon-induced surge heights along the west and south coasts. Additionally, comparing the return levels to those reported in previous studies, whereby extreme local SLR values were statistically obtained by using long-term observational data at the Yeosu, Tongyeong, and Busan tidal stations on the south coast (Kwon et al. 2009; Kang and Kim 2018; Kim and Suh 2018; respectively), the return period levels of the typhoon-induced surge height by both the GEV and Weibull distributions are overestimated. This comparison is summarized in Table 4. The return period levels by the GEV distribution are closer but higher than the mean values of the 100-year return period level. The Weibull distribution was applied to estimate the 50-year return period levels in previous studies (Kwon et al. 2009; Kang and Kim 2018). These values are also included in the ± 90% confidence intervals (CIs). However, as shown in Fig. 3, compared to the numerically obtained local extreme events, the return period levels by the GEV distribution tend to be underestimated. The estimated return period levels of the typhoon-induced surge height are much higher than the mean values of the observation data, which strongly supports the application of SLOSH model results in estimating the return period level of the typhoon-induced surge height. It is expected that this will promote the adoption of the return period level by policymakers and planners who require extreme values when making decisions for the prevention of coastal flooding, the management of coastal regions, or in response to climate change.

5 Conclusion

Climate change has led to increases in both the global mean and extreme sea levels. Although SLR values are increasing with similar patterns, the SLR rates of the seas around South Korea are much higher than the global mean SLR rate (KHOA; IPCC 2013). The typhoon-induced surge height is a main driver of extreme sea levels. As South Korea is increasingly exposed to typhoons that are becoming stronger and more frequently generated due to climate change, its coastal area is increasingly subject to local, meteorological SLR-related risks such as coastal flooding and inundation. Coastal management, policymaking, and planning with respect to SLR and climate change require the estimation of the probability of exceeding a certain level in any given year as the first step.

This research aims to estimate and update the local extreme SLR values induced by typhoons by implementing extreme value analysis with the GEV and Weibull distributions.

Table 4 Return period levels of the typhoon-induced surge height by the GEV and Weibull distributions and previous studies for verification purposes (unit: m)

Method or previous studies	Tidal station			
	Return period	Yeosu	Tongyeong	Busan
GEV	50	1.8	1.5	1.0
		95% CI: 1.0 (L)/3.7 (U)	95% CI: 0.8 (L)/2.9 (U)	95% CI: 0.6 (L)/1.9 (U)
	100	2.2	1.9	1.3
		95% CI: 1.1 (L)/5.4 (U)	95% CI: 1.0 (L)/4.2 (U)	95% CI: 0.7 (L)/2.6 (U)
Weibull	50	1.4	1.1	0.8
		95% CI: 1.4 (L)/1.4 (U)	95% CI: 1.1 (L)/1.2 (U)	95% CI: 0.8 (L)/0.9 (U)
	100	1.5	1.3	0.9
		95% CI: 1.5 (L)/1.6 (U)	95% CI: 1.2 (L)/1.3 (U)	95% CI: 0.9 (L)/0.9 (U)
Kim and Suh (2018)	50	–	0.9	0.6
	100	–	1.0	0.7
Kang and Kim (2018)	50	Mean: 1.3	Mean: 1.1	Mean: 0.6
		Standard deviation (STD): 0.5	STD: 0.3	STD: 0.2
	100	Mean: 1.7	Mean: 1.4	Mean: 0.9
		STD: 0.3	STD: 0.2	STD: 0.1
Kwon et al. (2006)	50	Mean: 1.4	Mean: 1.7	–
		90% CI: 0.9 (L)/2.9 (U)	90% CI: 0.9 (L)/5.9 (U)	
	100	Mean: 1.8	Mean: 2.4	–
		90% CI: 1.1 (L)/4.6 (U)	90% CI: 1.1 (L)/11.3 (U)	

To validate and select the best fitting curves of the annual maximum values obtained from the deterministic numerical SLOSH model, the Chi-S and K–S goodness-of-fit tests are employed. The statistical performance indicators, i.e., the weighted sum χ^2 of the Chi-S goodness-of-fit test and the supremum D_n of the K–S test, ascertain the acceptance of the null hypothesis, which validates the statistical analysis. These results also provide guidance for better estimations. The lower the statistical performance indicators are, the better the fitted curves are. As a result, the GEV distribution attained a better estimation of the return period levels of the typhoon-induced SLR. The GEV distribution tends to capture extreme values (please refer to Fig. 3 for details) and provides higher return period levels along the west and south coasts.

In addition, the return period levels of the typhoon-induced SLR by the GEV distribution conform better to the observation data than do the numerically obtained typhoon-induced surge heights in terms of extreme events. Even though its error ranges from ± 20 to ± 50%, the SLOSH model tends to overestimate the maximum wave height. (See Ku et al. 2019a, b for details.) The SLOSH model results based on the Korea input basin are suitable to estimate the return period level for coastal and risk management purposes. Additionally, the above numerical model covers all oceans of South Korea, and it provides the return period level at many more locations than just tidal stations recording the tidal level. This could be a useful tool or map for other purposes such as coastal management and related policymaking and planning.

Acknowledgements This study was funded by the Korea Ministry of Environment (MOE) as "Climate Change Correspondence Program (2014001310006)." The authors are grateful to the Korea Environment Institute for the administrative support on "Development of integrated model for climate change impact and vulnerability assessment and strengthening the framework for model implementation (2020-010-01(R))."

Author contributions H.K. and J.H.M. designed the analysis, analyzed the data, and wrote the manuscript. H.K. performed the analysis.

Funding This study was funded by the Korea Ministry of Environment (MOE) as the Climate Change Correspondence Program (20140013100006).

Data availability The authors confirm that the data supporting the findings of this study are available within the article and its supplementary materials. The data that support the extreme value analyses are available from the first author, H. Ku, upon reasonable request.

Code availability The methods described in this article were implemented using custom MATLAB (R2013b). Due to licensing restrictions by Korea Environment Institute, this code is not publicly available. Sea, Lake, and Overland Surges from Hurricanes (SLOSH) was acknowledged and provided by the National Oceanic and Atmospheric Administration (NOAA), an agency of the U.S. Department of Commerce to the corresponding author. Contact https://slosh.nws.noaa.gov/slosh/index.php for the software acknowledgement.

Compliance with ethical standards

Conflict of interest The authors declare no competing interests.

References

Ahrens CD (2005) Essentials of meteorology: an invitation to the atmosphere. Thomson Brooks/Cole, Belmont

Alam M, Emura K, Farnham C, Yuan J (2018) Best-fit probability distributions and return periods for maximum monthly rainfall in Bangladesh. Climate 6:9. https://doi.org/10.3390/cli6010009

Arns A, Wahl T, Dangendorf S, Jensen J (2015) The impact of sea level rise on storm surge water levels in the northern part of the German Bight. Coast Eng 96:118–131. https://doi.org/10.1016/j.coastaleng.2014.12.002

Boccotti P (2000) Wave mechanics for ocean engineering. Elsevier, The Netherlands

Butler A, Heffernan JE, Tawn JA, Flather RA, Horsburgh KJ (2007) Extreme value analysis of decadal variations in storm surge elevations. J Mar Syst 67:189–200. https://doi.org/10.1016/j.jmarsys.2006.10.006

Cazenave A, Cozannet GL (2014) Sea level rise and its coastal impacts. Earth's Fut 2:15–34. https://doi.org/10.1002/2013ef000188

Chen W-B, Lin L-Y, Jang J-H, Chang C-H (2017) Simulation of typhoon-induced storm tides and wind waves for the Northeastern coast of Taiwan using a tide-surge-wave coupled model. Water 9:594. https://doi.org/10.3390/w9070549

Dufour JM, Farhat A, Gardiol L, Khalaf L (1998) Simulation-based finite sample normality tests in linear regressions. Econom J 1:C154–C173. https://doi.org/10.1111/1368-423x.11009

Glahn B, Taylor A, Kurkowski N, Shaffer WA (2009) The role of the SLOSH model in national weather service storm surge forecasting. Natl Weather Dig 33:3–14

Goring DG, Stephens SA, Bell RG, Pearson CP (2011) Estimation of extreme sea levels in a tide-dominated environment using short data records. J Waterw Port Coast Ocean Eng 137:150–159. https://doi.org/10.1061/(asce)ww.1943-5460.0000071

Hamlington BD, Fasullo JT, Nerem RS, Kim KY, Landerer FW (2019) Uncovering the pattern of forced sea level rise in the satellite altimeter record. Geophys Res Lett 46:4844–4853. https://doi.org/10.1029/2018gl081386

Hay CC, Morrow E, Kopp RE, Mitrovica JX (2015) Probabilistic reanalysis of twentieth-century sea-level rise. Nature 517:481–484. https://doi.org/10.1038/nature14093

Hsiao S-C, Chen H, Chen W-B, Chang C-H, Lin L-Y (2019) Quantifying the contribution of nonlinear interactions to storm tide simulations during a super typhoon event. Ocean Eng 194:106661. https://doi.org/10.1016/j.oceaneng.2019.106661

Hsiao S-C, Wu H-L, Chen W-B, Chang C-H, Lin L-Y (2020) On the snesitivity of typhoon wave simulations to tidal elevation and current. J Marine Sci Eng 8:731. https://doi.org/10.3390/jmse8090731

IPCC (2013) Climate change 2013: the physical science basis. In: Stocker TF, Qin D, Plattner GK, Tignor M, Allen SK, Boschung J, Nauels A, Xia Y, Bex V, Midgley PM (eds) Contribution of working group I to the fifth assessment report of the intergovernmental panel on climate change. Cambridge University Press, Cambridge, p 1585

IPCC (2014) Climate change 2014: impacts, adaptation, and vulnerability. Part a: global and sectoral aspects. In: Field CB, Barros VR, Dokken DJ et al (eds) Contribution of working group II to the fifth assessment report of the intergovernmental panel on climate change. Cambridge University Press, Cambridge, p 1132

Jelesnianski C, Jye C, Shaffer W, Gilad A (1984) SLOSH—a hurricane storm surge forecast model. In: OCEANS 1984. IEEE, Washington, DC, pp 314–317

Jelesnianski CP, Chen J, Shaffer WA (1992) SLOSH: sea, lake, and overland surges from hurricanes. NOAA Technical Report NWS 48. National Oceanic and Atmospheric Administration, U. S. Department of Commerce, Silver Spring

Kang JW, Kim YS (2018) Estimation of extreme sea levels reflecting tide-surge characteristics. J Korean Soc Coast Ocean Eng 30:103–113. https://doi.org/10.9765/kscoe.2018.30.3.103

Ke Q, Jonkman S, van Gelder P, Bricker J (2018) Frequency analysis of storm-surge-induced flooding for the Huangpu River in Shanghai. China J Mar Sci Eng 6:70. https://doi.org/10.3390/jmse6020070

Kim Y, Cho K (2016) Sea level rise around Korea: analysis of tide gauge station data with the ensemble empirical mode decomposition method. J Hydro-environ Res 11:138–145. https://doi.org/10.1016/j.jher.2014.12.002

Kim HJ, Suh SW (2018) Improved hypothetical typhoon generation technique for storm surge frequency analyses on the Southwest Korean Coast. J Coast Res 85:516–520. https://doi.org/10.2112/si85-104.1

Kim SC, Chen J, Shaffer WA (1996) An operational forecast model for extratropical storm surges along the U.S. East Coast. In: Conference on oceanic and atmospheric prediction. American Meteorological Society Preprints, Atlanta, pp 281–286

Knutson TR, McBride JL, Chan J, Emanuel K, Holland G, Landsea C, Held I, Kossin JP, Srivastava AK, Sugi M (2010) Tropical cyclones and climate change. Nat Geosci 3:157–163. https://doi.org/10.1038/ngeo779

Kottegoda NT, Rosso R (1997) Statistics, probability, and reliability for civil and environmental engineers. McGraw-Hill, New York

Ku H, Maeng JH, Cho K (2019a) Climate change impact on typhoon-induced surges and wind field in coastal region of South Korea. J Wind Eng Ind Aerodyn 190:112–118. https://doi.org/10.1016/j.jweia.2019.04.018

Ku H, Maeng JH, Cho K (2019b) Deterministic estimation of typhoon-induced surges and inundation on Korean coastal regions. J Korean Soc Coast Ocean Eng 31:1–8. https://doi.org/10.9765/kscoe.2019.31.1.1

Kwon SJ, Park JS, Lee EI (2009) A study on the application of generalized extreme value distribution to the variation of annual maximum surge heights. J Korean Soc Coast Ocean Eng 21:241–253

Lowe JA, Woodworth PL, Knutson T et al (2010) Past and future changes in extreme sea levels and waves. In: Church JA, Woodworth PL, Aarup T, Wilson WS (eds) Understanding sea-level rise and variability. Blackwell, Chichester, pp 326–375

Panik MJ (2005) Advanced statistics from an elementary point of view. Elsevier, Amsterdam

Rao AD, Upadhaya P, Pandey S, Poulose J (2020) Simulation of extreme water levels in response to tropical cyclones along the Indian coast: a climate change perspective. Nat Hazards 100:151–172. https://doi.org/10.1007/s11069-019-03804-z

Seo J, Ku H, Cho K, Maeng JH, Lee H (2018) Application of SLOSH in estimation of typhoon-induced storm surges in the Coastal Region of South Korea. J Coast Res 85:551–555. https://doi.org/10.2112/si85-111.1

Shaffer W, Jelesnianski C, Chen J (1986) Hurricane storm surge forecasting. In: OCEANS'86. IEEE, Washington, DC, pp 1379–1385

Talke SA, Jay DA (2020) Changing tides: the role of natural and anthropogenic factors. Annu Rev Mar Sci 12:121–151. https://doi.org/10.1146/annurev-marine-010419-010727

Taylor A, Glahn B (2008) Probabilistic guidance for hurricane storm surge. In: 19th Conference on probability and statics. American Meteorological Society Preprints, New Oreleans, p 7.4

Toro GR, Resio DT, Divoky D, Niedoroda AW, Reed C (2010) Efficient joint-probability methods for hurricane surge frequency analysis. Ocean Eng 37:125–134. https://doi.org/10.1016/j.oceaneng.2009.09.004

Weather Meteorological Organization (2017) Catalysing innovation in weather science: WWRP implementation plan 2016–2023. Weather Meteorological Organization, Geneva

Woodworth PL, Menéndez M, Roland Gehrels W (2011) Evidence for century-timescale acceleration in mean sea levels and for recent changes in extreme sea levels. Surv Geophys 32:603–618. https://doi.org/10.1007/s10712-011-9112-8